The Astrophysical Journal Letters, 938:L18 (7pp), 2022 October 20 https://doi.org/10.3847/2041-8213/ac98ad

Prompt Emission of γ-Ray Bursts in the High-density Environment of Active Galactic Nucleus Accretion Disks

Davide Lazzati[1], Gustavo Soares[1], and Rosalba Perna[2,3]
[1] Department of Physics, Oregon State University, 301 Weniger Hall, Corvallis, OR 97331, USA; davide.lazzati@oregonstate.edu
[2] Department of Physics and Astronomy, Stony Brook University, Stony Brook, NY 11794-3800, USA
[3] Center for Computational Astrophysics, Flatiron Institute, New York, NY 10010, USA
Received 2022 August 14; revised 2022 September 28; accepted 2022 October 9; published 2022 October 18

Abstract

Long and short γ-ray bursts (GRBs) are traditionally associated with galactic environments, where circumburst densities are small or moderate (few to hundreds of protons per cubic centimeter). However, both are also expected to occur in the disks of active galactic nuclei, where the ambient medium density can be much larger. In this work we study, via semianalytical methods, the propagation of the GRB outflow, its interaction with the external material, and the ensuing prompt radiation. In particular, we focus on the case in which the external shock develops early in the evolution at a radius that is smaller than the internal shock one. We find that bursts in such high-density environments are likely characterized by a single, long emission episode that is due to the superposition of individual pulses, with a characteristic hard-to-soft evolution irrespective of the light-curve luminosity. While multipulse light curves are not impossible, they would require the central engine to go dormant for a long time before reigniting. In addition, short GRB engines would produce bursts with prompt duration that would exceed the canonical 2 s separation threshold and likely be incorrectly classified as long events, even though they would not be accompanied by a simultaneous supernova. Finally, these events have a large dynamical efficiency, which would produce a bright prompt emission followed by a somewhat dim afterglow.

Unified Astronomy Thesaurus concepts: Gamma-ray bursts (629); Galaxy accretion disks (562); Special relativity (1551)

1. Introduction

The disks of active galactic nuclei (AGNs), in addition to providing fuel to their central supermassive black holes (SMBHs), are also home to stars and the compact progenitors they leave behind. Stars are believed to exist in AGN disks due to two mechanisms: in situ formation from gravitational instabilities in the outer disk (e.g., Goodman 2003; Dittmann & Miller 2020) and capture from the nuclear star cluster surrounding the AGN (e.g., Artymowicz et al. 1993). The evolution of stars in these dense environments has been studied in detail in recent works (Cantiello et al. 2021; Dittmann et al. 2021; Jermyn et al. 2021). It has been shown that, in addition to growing to very large masses, AGN stars in the presupernova phase are fast rotators, which makes them ideal candidates as progenitors of long γ-ray bursts (GRBs; Jermyn et al. 2021).

Additionally, AGN disks are also conducive to the formation of short GRBs from binary neutron star (NS) mergers and possibly from NS–BH mergers with small enough mass ratios. This is due to the easiness of compact object binary formation in AGN disks. The NSs and BHs cluster in migration traps (e.g., Bellovary et al. 2016; McKernan et al. 2020), where binary formation via dynamical interactions is facilitated. Kinetic energy loss due to the interaction with the dense AGN disk medium further contributes to binary formation (Tagawa et al. 2020).

In addition to long and short GRBs, the disks of AGNs are expected to host a variety of other transients, from core-collapse supernovae (discussed by Grishin et al. 2021), to accretion-induced collapse of NSs (Perna et al. 2021b) and white dwarfs (Zhu et al. 2021b), to microtidal disruption events by stellar mass BHs (Yang et al. 2022). Some of these may also be accompanied by a relativistic jet and hence possibly emitting γ-ray photons. Even BH–BH mergers in AGN disks may have short GRB-like features (Bartos et al. 2017; see also Kaaz et al. 2021), as in the case of GW190521, which was modeled as due to the propagation of the binary through an AGN accretion disk (Graham et al. 2020). Proper identification of these transients, and hence help calibrating the number of stars and compact objects in AGN disks, bears numerous astrophysical implications. The AGN disks are a promising channel to explain some unexpected findings of the LIGO/Virgo data, such as BHs in the low-mass gap (Abbott et al. 2020a; Tagawa et al. 2020; Yang et al. 2020), as well as in the high-mass gap (Abbott et al. 2020b), and an asymmetry in the BH spin distribution (Callister et al. 2021; McKernan et al. 2022; Wang et al. 2021). Additionally, they can help constrain the neutrino background associated with relativistic sources (Fasano et al. 2021; Zhu et al. 2021a). As the prompt γ-ray emission is generally followed by longer-wavelength radiation, it would contribute to the AGN variability in the optical and infrared (Wang et al. 2022). With the upcoming Vera Rubin observatory, some of these transients will be observed; hence, it becomes especially important to recognize them in association with their prompt γ-ray emission.

The environment of AGN disks, due to its high density, can significantly change the appearance of a transient. Some of the general key features were discussed in Perna et al. (2021a). They showed how, depending on the mass of the SMBH (and hence of the AGN disk) and the location of the transient within the disk, GRBs and their afterglows can appear fully normal, diffused only at early times, or completely diffused at all

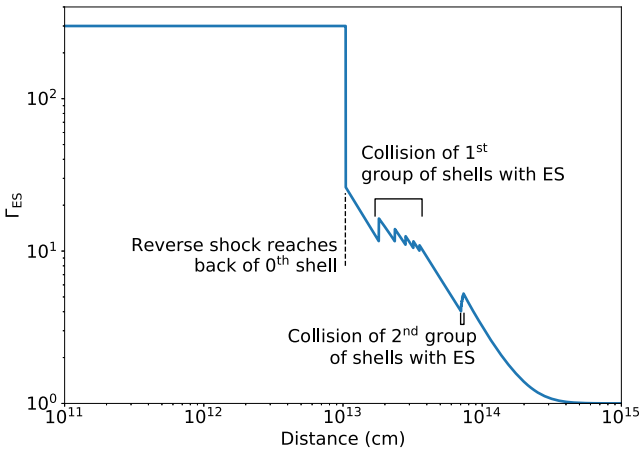

Figure 1. Dynamics of the externally shocked material as a function of the distance from the central engine. The fireball is the one that gave rise to the light curve in Figure 4.

wavelengths and observation times. For transients emerging from the innermost regions, the jet may be chocked before emerging from the disk photosphere (Zhu et al. 2021c).

From the GRB point of view, the existence of different classes of events is an observational requirement. Besides the classical short and long burst classification based on their T_{90} duration (Kouveliotou et al. 1993), there are at least two spectral classes within the long GRB population. Most spectra display a "tracking" behavior, in which the peak photon frequency tracks the light-curve luminosity. In a subset of cases, instead, the peak frequency consistently decreases in time, irrespective of what the luminosity does (e.g., Lu et al. 2012). The origin of such a duality is still debated, as are many of the key physical properties of the GRB prompt emission mechanism. In the following, we will argue that bursts exploding in high-density media are expected to display hard-to-soft spectral behavior and suggest observations to test this scenario. We will build on our previous work but focusing on a more in-depth study of the early phases of the jet, when the prompt emission is produced.

The paper is organized as follows. Section 2 describes our numerical methods and initial conditions. The simulation results are presented in Section 3, and we summarize and conclude in Section 4.

2. Methods

2.1. Qualitative Considerations

The prompt emission of GRBs, both long and short, is predominantly attributed to either the photospheric (Rees & Mészáros 2005; Pe'er et al. 2006; Giannios & Spruit 2007; Lazzati et al. 2009; Ryde et al. 2011) or internal shock (IS; Daigne & Mochkovitch 1998; Bošnjak et al. 2009) models, and it is likely that, at least in some cases, both mechanisms contribute to the observed radiation (Guiriec et al. 2011; Toma et al. 2011). If a GRB occurs in a low-density interstellar medium, the standard scenario is of a relativistic outflow that releases its internal energy as γ-ray radiation at a distance of $\sim 10^{13}$ cm from the engine. Only much farther out does the interstellar medium become relevant, causing the development of a forward/reverse shock system that powers the long-lasting afterglow emission (e.g., Mészáros & Rees 1997). In a high-density environment, on the other hand, the deceleration of the leading shell begins very early. In most cases, the photospheric emission is unaffected (Perna et al. 2021a, see their Figure 2), but there are many locations in the disk where the deceleration takes place earlier than the ISs, especially for the high range of central BH masses ($M_{\rm BH} > 10^7\ M_\odot$).

In this case, one can envisage that, since the deceleration of the leading shell is so sudden, the following shells catch up with the newly formed external shock (ES) very quickly. Instead of traditional ISs among shells, there would be shells colliding with the early formed ES. Such collisions would take place in a small range of radii, since the shells are moving at a much larger Lorentz factor than the ES, which is propagating in a high-density environment and therefore decelerating rapidly.

Some properties of the ensuing radiation pulses can be evaluated with simple considerations.

1. *If the central engine produces a set of similarly spaced shells, the pulses will merge, producing a single-episode prompt emission light curve*. Consider a shell that is released from the central engine at time t_i after the leading shell. If it collides at a distance $R_{\rm coll}$ with the decelerating leading shell, the ensuing emission is seen by an observer at time $R_{\rm coll}/c\Gamma_0^2$, where Γ_0 is the shell's Lorentz factor before the collision. The minimum duration of the emission is instead set by the angular timescale and driven by the Lorentz factor of the ES: $\Delta t_{\rm ang} = R_{\rm coll}/c\Gamma_{\rm ES}$. Since the collision can happen only if $\Gamma_0 > \Gamma_{\rm ES}$, we find that the pulse detection time (which is also the delay between the peaks from subsequent pulses) is shorter than the pulse duration. Shells emitted in a regular pattern, therefore, will produce pulses that overlap each other into a single, broad emission event. In order to observe a multipeaked light curve, a substantial engine dead time needs to be realized.
2. *The spectral evolution is hard to soft, irrespective of the light-curve flux*. Given the dynamics considerations discussed above, subsequent shells collide with the leading ES at increasing distances. The observed peak frequency of the synchrotron emission is inversely proportional to the collision distance (see, e.g., Equation (3) in Ghisellini et al. 2000), creating a systematic decrease of the peak frequency with time. This is at variance with respect to the standard IS scenario, in which the collision radii are expected to remain at a fairly constant distance from the engine throughout the burst prompt evolution. It should be noted that the observed synchrotron peak frequency also depends on the relative Lorentz factor between the shells. An engine that produces a shell with a large Lorentz factor at a late time could therefore cause a momentary increase in the peak frequency, overlaid on an overall decreasing trend. In particular, it can be expected that the peak frequency might increase after a long engine dead time, during which the ES significantly slowed to a lower Lorentz factor.
3. *The dynamical efficiency of the prompt emission is large*. The ISs are known to have low dynamical efficiency (Kobayashi et al. 1997; Lazzati et al. 1999), defined as the ratio of the energy that is dissipated in the shock over the total energy in the outflow. This is due to the fact that the relative velocity of the shells in ISs is mildly relativistic, since both shells are propagating at a large Lorentz factor in the same direction. In the case discussed here, instead, each shell collides with a large Lorentz factor against the decelerating ES, which is expect to be moderately relativistic ($\Gamma \sim 10$; see also Figure 1). As a

consequence, the dynamic efficiency is expected to be large. For a given radiative efficiency (the percentage of the dissipated energy that is radiated in electromagnetic waves), bursts in high-density media are therefore anticipated to be significantly brighter than those exploding in rarefied media.

4. *The broadband spectrum of the prompt emission is likely to be dominated by the self-synchrotron Compton (SSC) process*. This is the process in which the synchrotron photon created by the electron population is upscattered by another electron in the same population, shifting the peak in frequency by a factor γ_e^2. The importance of this process is quantified by the Compton parameter $Y = \tau_T \gamma_e^2$, the ratio between the total energy of the Comptonized photons over the total energy of the seed synchrotron photons. For a shell hitting the ES, we can evaluate the Compton parameter as $Y = \tau_T \gamma_e^2 \simeq 1836^2 R_{\rm ES} n_{\rm ISM} \sigma_T \Gamma_{\rm rel}^2/\Gamma$, where $\Gamma_{\rm rel}$ is the Lorentz factor of the shell in the frame of the ES, and Γ is the Lorentz factor of the merging shells in the laboratory frame. Assuming, as discussed above, that the ES does not move significantly from where it forms, we can substitute the expression for the thick shell ES radius (Sari & Piran 1995) and obtain

$$Y \simeq 10^{-4} E_{52}^{1/4} t_{\rm eng} \Gamma_2^{-1} n_{\rm ISM}^{3/4} \Gamma_{\rm rel}^2, \quad (1)$$

which is typically small for low-density external media but can be substantial for typical densities of AGN accretion disks.

2.2. Semianalytical Methods

In order to validate the qualitative considerations discussed above, we carried out semianalytical calculations of the evolution of a system of shells impacting a high-density external medium. The shells are ejected at small time intervals Δt from each other[4] from a central engine embedded in a uniform medium of number density $n_{\rm ISM} = 10^{12}$ cm^{-3}, typical of the central regions of AGN accretion disks (Thompson et al. 2005; Fabj et al. 2020). To keep the number of arbitrary assumptions at a minimum, we consider all shells ejected at regular intervals, and the thickness of each shell at ejection is set to $\Delta R = c\Delta t/2$. We also assume that all of the shells accelerate to the same asymptotic Lorentz factor $\Gamma_\infty = E/M_0 c^2$, where E is the energy of each shell, and M_0 is its rest mass.[5]

The first shell sweeps up the external medium. At the considered external densities and for typical shell thicknesses and energies, the shell deceleration takes place in the thick shell regime (Sari & Piran 1995). In this case, the ES radius is identified as the distance at which the reverse shock reaches the back of the shell. It reads

$$R_{\rm ES} = \left(\frac{3E\Delta t}{4\pi n_{\rm ISM} m_p c}\right)^{1/4} \simeq \simeq 4.7 \times 10^{13}\, E_{52}^{1/4} n_{\rm ISM,10}^{-1/4}, \Delta t^{1/4} \ \ {\rm cm}, \quad (2)$$

which, for our fiducial parameters, is smaller than the IS radius,

$$R_{\rm IS} = c\Delta t \Gamma_\infty^2 = 3 \times 10^{14}\, \Gamma_{\infty,2}^2 \Delta t. \quad (3)$$

A comparison of these equations reveals that the ES develops first if

$$n_{\rm ISM} > 6 \times 10^6\, E_{52}\, \Gamma_{\infty,2}^{-8}\, \Delta t^{-3} \qquad {\rm cm}^{-3}. \quad (4)$$

The further evolution of the ES is set by the amount of mass swept up according to Paczynski & Rhoads (1993),

$$\Gamma = \frac{\Gamma_\infty + f}{\sqrt{1 + 2\Gamma_\infty f + f^2}}, \quad (5)$$

were f is the fraction of the swept-up mass over the rest mass of the first shell.

Simple kinematics equations can be used to determine the time $t_{\rm coll}$ and radius $R_{\rm coll}$ at which the second shell collides with the ES formed by the first shell. The impact of the shell creates a prompt emission spike during a short transient in which a reverse shock propagates backward into the shell. After that, the ES is reenergized, and its velocity increases according to

$$\beta_{\rm after\ collision} = \frac{\beta_{\rm shell} M_0 \Gamma_\infty + \beta_{\rm ES} M_{\rm ISM}(R_{\rm coll}) \Gamma_{\rm ES}}{M_0 \Gamma_\infty + M_{\rm ISM}(R_{\rm coll}) \Gamma_{\rm ES}}, \quad (6)$$

where $\beta_{\rm after\ collision} c$ is the velocity of the ES immediately after the collision, $\beta_{\rm shell} c = \sqrt{1 - 1/\Gamma_\infty^2}\, c$ is the velocity of the incoming shell, $\beta_{\rm ES} c$ is the velocity of the ES immediately before the collision, $M_{\rm ISM}(R_{\rm coll})$ is the mass swept up by the ES at the collision radius, and $\Gamma_{\rm ES}$ is the Lorentz factor of the ES immediately before the collision. After the extra energy injection, the ES settles back into its self-similar evolution, with a Lorentz factor set again by Equation (5), albeit with a higher value of M_0. Subsequent shells have the same effect, and their collision radii and kinematics can be calculated analogously.

As discussed above, for a short time during the collision, a reverse shock forms into the shell, which can give rise to γ-ray emission. We calculate the properties of the emission following the standard synchrotron IS methods (e.g., Piran 2004), which we briefly summarize here. Electrons are accelerated to an internal Lorentz factor $\gamma_{\rm inj} = \Gamma_{\rm rel} \epsilon_e m_p/m_e$, and a random, small-scale magnetic field is generated with intensity $B = \sqrt{2\epsilon_B \Gamma_{\rm rel} M_0 c^2/(R_{\rm collision}^2 \Gamma_\infty \Delta t\, c)}$. This gives rise to synchrotron emission with a spectrum that peaks at an observed frequency

$$\nu_{\rm syn,obs} = \frac{2e}{3\pi m_e\, c} \gamma_{\rm inj}^2 B \Gamma_{\rm after\ collision}. \quad (7)$$

As shown above, the conditions of the material favor a very intense SSC radiation component (see, e.g., Marscher & Gear 1985). This has two important consequences. First, the real peak of the emission is at much higher frequencies, $\nu_{\rm SSC,obs} = \gamma_{\rm inj}^2 \nu_{\rm syn,obs}$.[6] Second, the electrons cool very rapidly,

[4] We consider an engine that ejects a shell of width $c\Delta t/2$, turns off for a time interval $c\Delta t/2$, and repeats periodically.

[5] Note that in traditional IS studies, the shells are required to have different Lorentz factors to allow for internal collisions. Since in this study, we concentrate on collisions of the shells with the ES, there is no need to postulate a dispersion of Lorentz factors.

[6] However, such a high-frequency peak might be missed in observations due to a lack of instrument sensitivity and/or because the high-energy photons are absorbed in photon–photon interactions either internally in the fireball or with the radiation field.

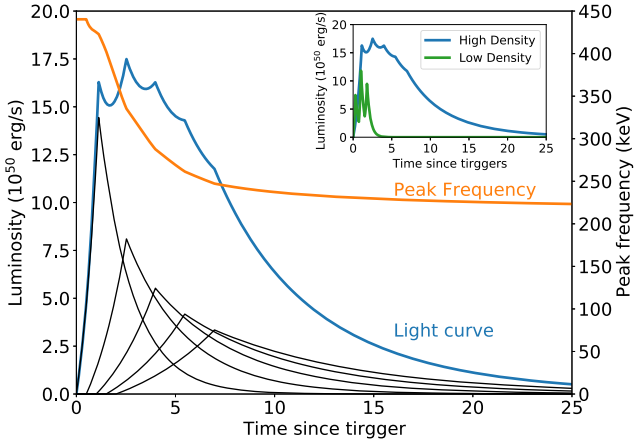

Figure 2. Simulated light curve and peak frequency evolution for a burst exploding in a high-density medium $n_{\rm ISM} = 10^{12}$ cm^{-3}. The fireball is made with an initial shell at $t = 0$ followed by five equally spaced additional shells ($\Delta t = 0.5$ s). The individual pulses from the five collisions are shown with black lines, while the overall pulse profile is shown with a blue line. The orange line instead shows the evolution of the peak frequency of the spectrum (excluding SSC; see right y-axis). The inset shows a comparison between the prompt light curve (blue) and the prompt emission of an analogous fireball exploding in a low-density environment and therefore powered by ISs.

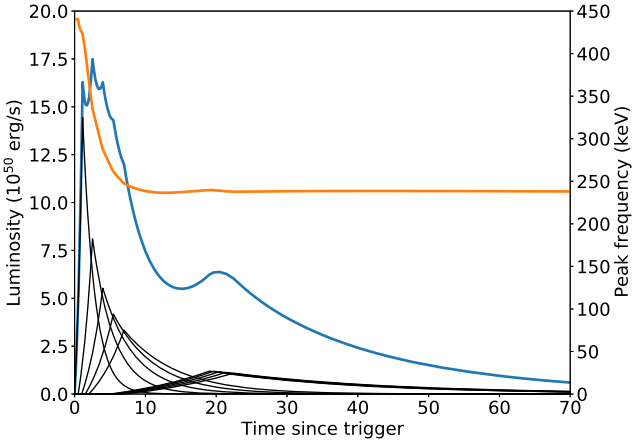

Figure 3. Same as Figure 2 but for a central engine that turns back on after a long pause of 5 s, ejecting another five shells analogous to the initial ones.

and the pulse duration is therefore expected to be driven by the fireball curvature, yielding an observed pulse with

$$\Delta t_{\rm pulse} = \frac{R_{\rm collision}}{c\Gamma^2_{\rm after\ collision}}. \quad (8)$$

The set of equations described here cannot be solved analytically for repeated impacts but can be easily implemented in a computer program. In the following section, we show some examples of predicted light curves and spectra.

3. Results

Figure 1 shows the dynamical evolution of an outflow made of two shell groups impacting on a high-density external medium ($n_{\rm ISM} = 10^{12}$ cm^{-3}). The graph shows the Lorentz factor of the outflow as a function of distance, with discontinuities marking the times at which shell collisions take place. In detail, the figure shows an outflow made by 11 shells. The first is emitted by the central engine at time $t = 0$, followed by five that are emitted at 0.5 s intervals ($\Delta t = 0.5$ s). Subsequently, the engine goes dormant for 20 s, and it eventually ejects a second group of shells identical to the initial ones. The dynamics of the outflow is as follows. Initially, the first shell coasts until it develop an external forward/reverse shock system. When the reverse shock reaches the back of the first shell, a significant drop in Lorentz factor is seen in the figure, at approximately $r = 10^{13}$ cm. The Lorentz factor subsequently decreases steadily due to the accumulation of ambient material by the forward shock until the second shell reaches the ES and a sudden increase in Lorentz factor is observed. This sequence repeats for all subsequent shells, albeit with an overall decreasing trend. Note, however, that when the second set of shells impacts the ES, they are so close to each other that their individual effect is difficult to discern.

Figure 2 shows the light curve and peak frequency evolution of a GRB exploding into a high-density medium with $n_{\rm ISM} = 10^{12}$ cm^{-3}. The burst is made of six shells, all with the same characteristics in terms of mass, energy ($E_{\rm shell} = 10^{52}$ erg), Lorentz factor ($\Gamma_\infty = 300$), width, and separation from one another ($\Delta t = 0.5$ s).[7] The figure reveals some interesting features. As expected from the qualitative discussion in Section 2.1, the individual pulses (shown with black lines) are separated by a time interval that is significantly shorter than their duration and therefore merge in a single broad envelope (blue line). In addition, later collisions give rise to longer pulses with lower peak frequency; therefore, the overall integrated pulse assumes a fast rise and exponential decay (FRED) shape known to occur in GRBs[8] (Fenimore et al. 1996; Daigne & Mochkovitch 1998). The spectral evolution also confirms the qualitative prediction and is overall hard to soft, irrespective of the light-curve luminosity evolution. These bursts would therefore be outliers to the Golenetskii correlation (Golenetskii et al. 1983), which predicts a tight correlation between luminosity and peak frequency. In the inset, we compare the overall light curve to the prompt emission of an analogous burst that exploded in an interstellar medium with low density ($n_{\rm ISM} < 10^4$ cm^{-3}; green line). In this case, the emission is powered by ISs, and the shells were injected with random Lorentz factors between $\gamma_{\rm min} = 10$ and $\Gamma_{\rm max} = 190$. The light curve (shown in green) is characterized by three individual pulses and has an overall duration comparable to the engine active time. The two fireballs contain the same energy, but the IS-powered light curve is much less energetic, confirming our qualitative estimate that light curves in high-density media would be more energetic. Finally, albeit not shown in the figure, the peak frequency of the second pulse of the IS-powered light curve is larger than that of the first and third pulses, making it a spectrally tracking burst.

Figure 3 explores a slightly more complex scenario, in which the burst's central engine goes dormant for a long time compared to the separation between consecutive shells. In particular, the burst in the figure starts analogously to the one in Figure 2, stops for 5 s (10 times longer than the intershell separation), and restarts afterward by emitting another series of five shells identical to the initial ones. As can be seen by inspecting the figure, a second broad peak appears at about 20 s, again made by the superposition of the individual pulses. Since by that time, the duration of the individual pulses is much

[7] The time delay among shells is reflected in the start time of the pulses in the figures. The pulse peak time is instead set by the pulse duration, which we assumed to be the angular timescale (see also the first item in Section 2.1).

[8] Note, however, that the so-called FRED shape can be due to a variety of effects and is not a unique prediction of this model.

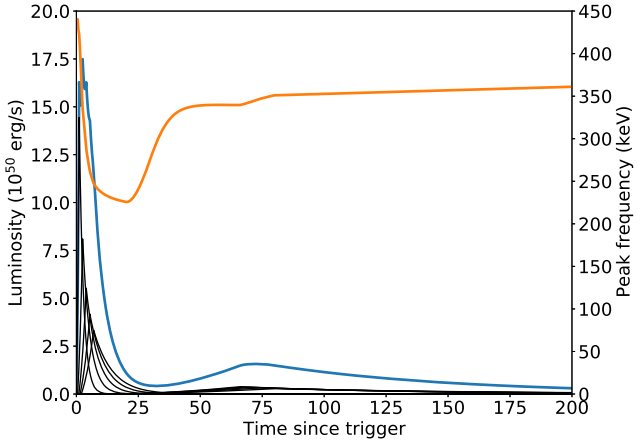

Figure 4. Same as Figures 2 and 3 but for a central engine with an even longer pause of 20 s. In this case, the peak frequency of the second pulse shows an increase with respect to the one at the end of the first pulse.

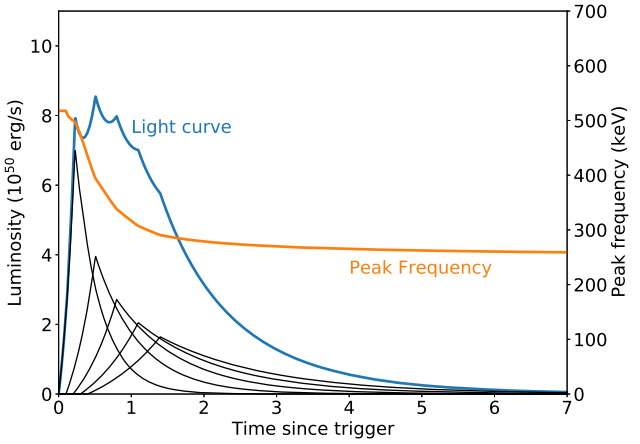

Figure 5. Same as Figures 2, 3, and 4 but for a central engine with a short activity that mimics a short GRB. The case shown is for an engine that releases shells at 0.1 s intervals ($\Delta t = 0.1$ s). Despite the short duration of the engine activity ($T_{\rm eng} = 0.55$ s), the prompt light curve has a duration of $T_{90} = 3.7$ s, placing this event firmly in the long burst category.

longer than the interpulse separation, the spectral evolution is all but gone, except for a small hint of hardening of the spectrum in correspondence with the peak of the second pulse.

In Figure 4, we explore the case of an even longer dead time (20 s), so that two well-separated pulses can be seen in the light curve. This burst is the one shown in the dynamical example of Figure 1. In this case, the ES has had enough time to slow down considerably by the time the late shells impact. Because of that, the $\gamma^2_{\rm inj} \propto \Gamma^2_{\rm rel}$ term in Equation (7) dominates, causing a hardening of the spectrum. For the same reason noted in the previous case, however, the spectral evolution is suppressed at late times, after the initial hardening, when the second set of shells impacts the ES.

An additional consideration can be made for the case of short GRBs. In the standard IS or photospheric scenarios, the duration of the prompt emission (usually characterized through the T_{90} parameter) corresponds to the duration of the engine activity. In the scenario considered here, however, the duration of a pulse is set by the curvature constraint and becomes larger for later pulses. The duration of the prompt emission is therefore potentially longer than the engine duration, and a short GRB engine may produce a burst with prompt emission lasting longer than the canonical 2 s and therefore identified as a long burst. To check this possibility, we show in Figure 5 the result of our model for an engine that releases an initial shell at $t = 0$ followed by five additional shells at 0.1 s intervals ($\Delta t = 0.1$ s). The total duration of the engine activity is therefore $T_{\rm eng} = 0.55$ s, placing this engine in the short GRB family. As anticipated, the resulting light curve has a much longer duration, $T_{90} = 3.7$ s, which would cause the incorrect identification of this event as a long-duration GRB.

4. Discussion and Conclusions

We have presented a qualitative and semianalytic study of the prompt emission from GRBs exploding in high-density media. In particular, we have focused on the consequence of the fact that, for densities larger than $\sim 10^6$ cm^{-3}, the ES develops before the ISs take place. As a consequence, the light curve is powered by a succession of shells impacting the forming ES, each generating a strong shock system with a large Lorentz factor contrast. This is different from the IS case, in which mild shocks with moderate Lorentz factor contrast form due to the collisions between pairs of shells before the ES develops.

The main conclusion of our study is the prediction that bursts from high-density environments, like those that characterize the accretion disks of AGNs, should have single broad pulses with a FRED shape, and that their spectral evolution should be hard to soft. Hard-to-soft spectral evolution is observed in GRB light curves (e.g., Lu et al. 2012), and its origin is still debated. In our model, it is due to the fact that the FRED pulse is a superposition of shorter pulses, each of them with a decreasing peak frequency due to the increasing distance at which they are produced. While more complex light curves are possible, they require the central engine to become dormant for a period of time that is orders of magnitude longer than the initial intershell separation, an occurrence that appears rare if not at all unlikely. In addition, the dynamical efficiency of bursts exploding in high-density media is larger than for traditional ISs, owing to the larger Lorentz factor contrast. In the cases shown in the figures, all bursts have dynamical efficiencies larger than 90%, compared to an efficiency of 9% for the IS comparison in the inset of Figure 2. Finally, the prompt emission duration is found to exceed 2 s even for short burst engines, therefore opening the possibility that some short GRBs from high-density environment have been incorrectly classified as long bursts. Some bursts with long duration have indeed defied classification due to the lack of a supernova component. Two well-studied cases (GRB 060505 and GRB 060614; Della Valle et al. 2006; Fynbo et al. 2006; Gal-Yam et al. 2006; Gehrels et al. 2006), however, cannot be due to bursts from AGN accretion disks due to the complexity of their prompt light curve and location outside of the center of their host galaxies. The case of GRB 111005A (MichałowskI et al. 2018) is more interesting. The burst was classified as a long event with a single broad pulse, did not have an associated supernova, and was located within 1″ of the center of its host galaxy. However, it was subenergetic, and the data quality did not allow for a spectral study of the prompt emission. GRB 111005A therefore makes a good candidate for a GRB powered by a binary NS merger within an AGN accretion disk, but the low energetics and possible small offset from the center of the galaxy deserve further investigation.

This model can be tested against a series of predictions and implications. First, hard-to-soft bursts should be predominantly FREDs, possibly showing evidence of variability overlaid on the overall pulse profile. Second, if an afterglow is observed from such bursts, it should show the characteristics of high external density, such as a fast evolution and a spectrum characterized by high-frequency self-absorption (Wang et al. 2022). Finally, should a precise localization be available, the burst should originate from the very center of the host galaxy.

The study presented here is based on a series of simplifications that deserve further study and are summarized and commented upon in the following.

1. We have assumed that individual pulses from the collision of a shell with the ES have no internal spectral evolution. Since electrons are expected to cool quickly, the pulse duration is expected to be due to the curvature of the shell, making this assumption reasonable. Peak evolution of order of a factor of $\sim$2 between the beginning and end of each pulse is, however, likely present due to the change in the angle between the line of sight to the observer and the local outflow velocity.
2. We have assumed that the prompt emission is entirely due to the synchrotron mechanism. However, there is convincing evidence that photospheric emission is at least contributing to the prompt emission in many bursts (Rees & Mészáros 2005; Pe'er et al. 2006; Giannios & Spruit 2007; Lazzati et al. 2009; Guiriec et al. 2011; Ryde et al. 2011; Toma et al. 2011). Neglecting photospheric emission as a first-order approximation is justified here by the fact that the shocks we consider have a large Lorentz factor contrast and therefore are very efficient compared to ISs that are expected to have small radiative efficiency (Kobayashi et al. 1997; Lazzati et al. 1999).
3. With the aim of minimizing any arbitrary choice of parameters, we have considered an outflow made of identical shells. While this choice allows for robust conclusions and predictions, it may overlook important features of the light curves and spectra. In particular, it is unlikely that an engine that has stopped producing an outflow for a long time (like those shown in Figures 3 and 4) will turn on at a late time, producing shells with the same properties as those in the initial phase. If later shells have lower luminosities or Lorentz factors, for example, different temporal and spectral evolution would be expected. This scenario should be studied with the aid of a physical model for the outflow generation from the central engine.
4. Perhaps the most important simplification we have adopted is to limit our discussion of the SSC component. In a simple scenario, the peak of the SSC emission is at a frequency that is $\gamma_{\rm inj}^2$ larger than the synchrotron peak. In our case, that is likely in the GeV or TeV bands, well above the frequencies at which GRBs are detected and studied. It is possible, however, that significant feedback develops if even a fraction of these high-energy photons are scattered backward in the high-density ambient material (see, for example, Beloborodov 2005a, 2005b). The ensuing spectral modifications, however, are difficult to predict in a general case and would require a more refined model of both the outflow and the external medium. Both of these are beyond the scope of this work.
5. Finally, we would like to mention that our external medium model might be oversimplified. On the one hand, the vertical structure of an AGN accretion disk is Gaussian and not constant (Sirko & Goodman 2003; Thompson et al. 2005). On the other hand, there may be significant modifications due to the per-explosion stellar and binary evolution as a result of radiation pressure, winds, feedback from accretion, etc. (Kimura et al. 2021; Tagawa et al. 2022; Yuan et al. 2022).

We would like to thank the anonymous referee for the constructive review and suggestions that led to a significant improvement of this paper. D.L. and G.S. acknowledge support from NSF award AST-1907955. R.P. acknowledges support by NSF award AST-2006839.

ORCID iDs

Davide Lazzati https://orcid.org/0000-0002-9190-662X
Gustavo Soares https://orcid.org/0000-0002-6569-5769
Rosalba Perna https://orcid.org/0000-0002-3635-5677

References

Abbott, B. P., Abbott, R., Abbott, T. D., et al. 2020a, ApJL, 892, L3
Abbott, R., Abbott, T. D., Abraham, S., et al. 2020b, PhRvL, 125, 101102
Artymowicz, P., Lin, D. N. C., & Wampler, E. J. 1993, ApJ, 409, 592
Bartos, I., Kocsis, B., Haiman, Z., & Márka, S. 2017, ApJ, 835, 165
Bellovary, J. M., Mac Low, M.-M., McKernan, B., & Ford, K. E. S. 2016, ApJL, 819, L17
Beloborodov, A. M. 2005a, ApJL, 618, L13
Beloborodov, A. M. 2005b, ApJ, 627, 346
Callister, T. A., Haster, C.-J., Ng, K. K. Y., Vitale, S., & Farr, W. M. 2021, ApJL, 922, L5
Cantiello, M., Jermyn, A. S., & Lin, D. N. C. 2021, ApJ, 910, 94
Bošnjak, Ž., Daigne, F., & Dubus, G. 2009, A&A, 498, 677
Daigne, F., & Mochkovitch, R. 1998, MNRAS, 296, 275
Della Valle, M., Chincarini, G., Panagia, N., et al. 2006, Natur, 444, 1050
Dittmann, A. J., Cantiello, M., & Jermyn, A. S. 2021, ApJ, 916, 48
Dittmann, A. J., & Miller, M. C. 2020, MNRAS, 493, 3732
Fabj, G., Nasim, S. S., Caban, F., et al. 2020, MNRAS, 499, 2608
Fasano, M., Celli, S., Guetta, D., et al. 2021, JCAP, 2021, 044
Fenimore, E. E., Madras, C. D., & Nayakshin, S. 1996, ApJ, 473, 998
Fynbo, J. P. U., Watson, D., Thöne, C. C., et al. 2006, Natur, 444, 1047
Gal-Yam, A., Fox, D. B., Price, P. A., et al. 2006, Natur, 444, 1053
Gehrels, N., Norris, J. P., Barthelmy, S. D., et al. 2006, Natur, 444, 1044
Ghisellini, G., Celotti, A., & Lazzati, D. 2000, MNRAS, 313, L1
Giannios, D., & Spruit, H. C. 2007, A&A, 469, 1
Golenetskii, S. V., Mazets, E. P., Aptekar, R. L., & Ilinskii, V. N. 1983, Natur, 306, 451
Goodman, J. 2003, MNRAS, 339, 937
Graham, M. J., Ford, K. E. S., McKernan, B., et al. 2020, PhRvL, 124, 251102
Grishin, E., Bobrick, A., Hirai, R., Mandel, I., & Perets, H. B. 2021, MNRAS, 507, 156
Guiriec, S., Connaughton, V., Briggs, M. S., et al. 2011, ApJL, 727, L33
Jermyn, A. S., Dittmann, A. J., Cantiello, M., & Perna, R. 2021, ApJ, 914, 105
Kaaz, N., Schrøder, S. L., Andrews, J. J., Antoni, A., & Ramirez-Ruiz, E. 2021, arXiv:2103.12088
Kimura, S. S., Murase, K., & Bartos, I. 2021, ApJ, 916, 111
Kobayashi, S., Piran, T., & Sari, R. 1997, ApJ, 490, 92
Kouveliotou, C., Meegan, C. A., Fishman, G. J., et al. 1993, ApJL, 413, L101
Lazzati, D., Ghisellini, G., & Celotti, A. 1999, MNRAS, 309, L13
Lazzati, D., Morsony, B. J., & Begelman, M. C. 2009, ApJL, 700, L47
Lu, R.-J., Wei, J.-J., Liang, E.-W., et al. 2012, ApJ, 756, 112
Marscher, A. P., & Gear, W. K. 1985, ApJ, 298, 114
McKernan, B., Ford, K. E. S., Callister, T., et al. 2022, MNRAS, 514, 3886
McKernan, B., Ford, K. E. S., & O'Shaughnessy, R. 2020, MNRAS, 498, 4088
Mészáros, P., & Rees, M. J. 1997, ApJ, 476, 232
MichałowskI, M. J., Xu, D., Stevens, J., et al. 2018, A&A, 616, A169
Paczynski, B., & Rhoads, J. E. 1993, ApJL, 418, L5
Pe'er, A., Mészáros, P., & Rees, M. J. 2006, ApJ, 642, 995
Perna, R., Lazzati, D., & Cantiello, M. 2021a, ApJL, 906, L7

Perna, R., Tagawa, H., Haiman, Z., & Bartos, I. 2021b, ApJ, 915, 10
Piran, T. 2004, RvMP, 76, 1143
Rees, M. J., & Mészáros, P. 2005, ApJ, 628, 847
Ryde, F., Pe'er, A., Nymark, T., et al. 2011, MNRAS, 415, 3693
Sari, R., & Piran, T. 1995, ApJL, 455, L143
Sirko, E., & Goodman, J. 2003, MNRAS, 341, 501
Tagawa, H., Haiman, Z., & Kocsis, B. 2020, ApJ, 898, 25
Tagawa, H., Kimura, S. S., Haiman, Z., et al. 2022, ApJ, 927, 41
Thompson, T. A., Quataert, E., & Murray, N. 2005, ApJ, 630, 167
Toma, K., Wu, X. F., & Mészáros, P. 2011, MNRAS, 415, 1663
Wang, Y.-H., Lazzati, D., & Perna, R. 2022, MNRAS, 516, 5935
Wang, Y.-H., McKernan, B., Ford, S., et al. 2021, ApJL, 923, L23
Yang, Y., Bartos, I., Fragione, G., et al. 2022, ApJL, 933, L28
Yang, Y., Gayathri, V., Bartos, I., et al. 2020, ApJL, 901, L34
Yuan, C., Murase, K., Guetta, D., et al. 2022, ApJ, 932, 80
Zhu, J.-P., Wang, K., & Zhang, B. 2021a, ApJL, 917, L28
Zhu, J.-P., Yang, Y.-P., Zhang, B., et al. 2021b, ApJL, 914, L19
Zhu, J.-P., Zhang, B., Yu, Y.-W., & Gao, H. 2021c, ApJL, 906, L11